Journal of Environmental Health Science and Engineering (2020) 18:515–529
https://doi.org/10.1007/s40201-020-00479-8

RESEARCH ARTICLE

Modeling of chromium (VI) removal from aqueous solution using modified green-Graphene: RSM-CCD approach, optimization, isotherm, and kinetic studies

Allahbakhsh Javid[1] · Aliakbar Roudbari[1] · Nader Yousefi[2] · Mohammad Alizadeh Fard[3] · Brian Barkdoll[3] · Seyedeh Solmaz Talebi[4] · Saeed Nazemi[1] · Marjan Ghanbarian[1] · Seid Kamal Ghadiri[1]

Received: 23 October 2019 / Accepted: 14 April 2020 / Published online: 6 May 2020

Abstract

Background The aim of this study was to investigate the removal of Cr (VI) using Green-Graphene Nanosheets (GGN) synthesized from rice straw.

Methods Synthesis of the GGN was optimized using response surface methodology and central composite design (CCD). The effect of two independent variables including KOH-to-raw rice ash (KOH/RRA) ratio and temperature on the specific surface area of the GGN was determined. To have better removal of Cr (VI), GGN was modified using the grafting amine group method. In the Cr (VI) removal process, the effects of four independent variables including initial Cr (VI) concentration, adsorbent dosage, contact time, and initial solution pH were studied.

Results The results of this study showed that the optimum values of the KOH/RRA ratio and temperature for the preparation of GGN were 10.85 and 749.61 °C, respectively. The maximum amount of SSA obtained at optimum conditions for GGN was 551.14 ± 3.83 m 2 /g. The optimum conditions for Cr (VI) removal were 48.35 mg/L, 1.46 g/L, 44.30 min, and 6.87 for Cr (VI) concentration, adsorbent dosage, contact time, and pH, respectively. Based on variance analysis, the adsorbent dose was the most sensitive factor for Cr (VI) removal. Langmuir isotherm (R2 = 0.991) and Pseudo-second-order kinetic models (R2 = 0.999) were the best fit for the study results and the Q max was 138.89 mg/g.

Conclusions It can be concluded that the predicted conditions from the GGN synthesis model and the optimum conditions from the Cr (VI) removal model both agreed with the experimental findings.

Keywords Chromium (VI) adsorption · Rice straw · Green-Graphene · Response surface methodology · Isotherm and kinetic study

Introduction

Discharge of industrial wastewater as a consequence of the rapid growth of population and manufacturing has deteriorated the quality of aquatic systems. Wastewater containing contaminants such as heavy metals could threaten aquatic biota and human health due to their persistence and toxicity [1, 2]. Chromium is one of the most important toxic contaminants which has been discharged into the environment. The effluents of tanneries, cement ceramics and mining, electroplating and power generation industries, metal, paint and wood processing, chrome plating, battery manufacturing, and plastic manufacturing units could comprise various concentrations of chromium higher than the discharged limits [3–5].

Chromium has a high melting point and is a lustrous metal that has various forms in the environment. Trivalent and hexavalent chromium are the most common oxidation forms of chrome [2, 6]. Hexavalent chromium is discharged to the environment via many industries and shows serious threats to humans and the environment even at low concentrations. Hexavalent chromium can be accumulated in the food chain and its excessive intake can cause cancer, inherited gene

✉ Seid Kamal Ghadiri
kamalgh2005@gmail.com

[1] Department of Environmental Health Engineering, School of Public Health, Shahroud University of Medical Sciences, Shahroud, Iran

[2] Department of Environmental Health Engineering, School of Public Health, Tehran University of Medical Sciences, Tehran, Iran

[3] Department of Civil and Environmental Engineering, Michigan Technological University, Houghton, MI, USA

[4] Department of Epidemiology, School of Medicine, Shahroud University of Medical Sciences, Shahroud, Iran

defects, cytotoxic and mutagenic nervous system failure, and liver and kidney damage [1, 5, 7]. Therefore, stringent standards have been considered for chromium in the water. For drinking waters, the maximum allowable of total chromium concentration is 100 and 50 ppb based on the standard of environmental protection agency (EPA) and EU directive for potable water standards, respectively. Thus, the elimination of Cr (VI) from water is crucial due to its toxicity and mobility [2, 8]. There are various technologies for the elimination of chromium from water such as catalytic degradation, ion exchange, membrane filtration, chemical precipitation, electrotransformation, lime coagulation, and adsorption [2, 5, 8]. Nonetheless, production of toxic metallic sludge, the high operational cost of physicochemical processes and low efficiency of membrane filtration and ion exchange especially at low concentrations lead to the consideration of other alternatives for chromium removal [5, 9].

The adsorption process has been greatly employed for the removal of chromium because of the eco-friendliness properties, simplicity of design and, low-cost process in comparison with conventional methods [10]. Application of various simple and bio-resource adsorbents have been elucidated for removal of chrome [11]. Nevertheless, new adsorbents are still under study to increase the adsorption capacity and minimize disposal problems.

Graphene and carbon nanotubes (CNTs) are new members of the category of the carbon-based family which are common than other adsorbents to remove various contaminants [12, 13]. Having high adsorption capacity and employing different materials as functional groups make graphene an effective matter for adsorbing chromium from drinking water [14]. Graphene oxide (GO) include various functional groups contain oxygen such as amine, epoxide, and hydroxyl on the basal plane and groups of carboxyl and carbonyl located on the edge planes [15, 16]. These functional groups are responsible for the production of the large negative charged surface on the GO that is the main factor for effective adsorption of positively charged materials like metal ions [17] and insignificant adsorption of anionic agents [18]. On the other hand, because of the π–π interactions between neighboring layers of GO, agglomeration and restacking of its layers during utilization are problems leading to lower effective surface area and adsorption capacity of GO than expected [19]. These problems can be overcome through the use of reduced graphene oxide (rGO) [20]. rGO has been suggested as a better adsorbent for anionic agents due to a lower negative charge than graphene oxide [18]. Recently, rGO has been generated by the activation of biomass resources using potassium hydroxide as alkaline activator and process of the carbonization [21–23]. Notwithstanding the advances attained, there is no investigation on the optimization of the parameters affecting the synthesis of rGO.

Rice straw is an agricultural byproduct with negligible nutritional value for livestock and could be applied as fuel, building construction material (thatching), and livestock bedding or basket making. In Iran, more than 2.2 Mt of rice are annually produced (in 2008) and their straw is mostly burned for the purposes of quick volume reduction of the waste, disposal and immediate land clearing [24]. Therefore, rice straw could be chosen as an inexpensive material for the production of graphene-based adsorbents using a cost-effective and simple pathway named Thermo-Chemical Reduction (TCR).

Among several different experimental designs in response surface methodology as statistical approach, central composite design (CCD) model is most common method to investigate individual and combined effects of independent parameters on response variable due to the simple structure, higher number of degrees of freedom and high efficiency and can produce comparably good results with the least number of experiments [25–27].

In the present study, the optimal fabrication condition for the preparation of a Green-Graphene Nanosheet (GGN) from rice straw was uniquely investigated using response surface methodology (RSM) according to the five-level two-factor CCD approach. In addition, after modification using the grafting amine group method the final product was employed at optimal values of parameters for hexavalent chromium removal from water for the first time.

Materials and methods

Materials

All materials employed (used without purification) in the present work i.e., ethanol, potassium hydroxide, and potassium dichromate were purchased from Sigma-Aldrich Co, USA. Sodium hydroxide and hydrochloric acid were obtained from the Merck Company (Darmstadt, Germany). It merits mentioning that all chemicals applied in the experiments were analytical grade.

Preparation of the adsorbent

Primary stage

Rice straws were obtained from a rice field in Ghaemshahr city, Mazandaran, Iran. The samples were transferred to the lab and washed thoroughly with deionized water for the removal of impurities. The samples were dried for 4 h at 105 °C and 10 g of dried product was added to a glass flask with 500 mL of ethanol (50%) solution. Then, the mixture was agitated using a sonication device at 35 kHz for 0.5 h. Then, the product was filtrated and dried 4 h at 105 °C. Thereafter, the sample was combusted at 280 °C for 25 min to achieve raw rice ash (RRA). Finally, at the end of the primary stage,

the RRA was sieved and ground to achieve the appropriate size of a number < 149 μm (100 mesh).

Experimental design for the production of GGN

Central Composite Design (CCD) method was employed to specify the best condition for GGN production and optimization of the process [28]. RSM was employed as a statistical, design and modeling technique to minimize experimental numbers [29–31]. It evaluates the interaction effects of KOH/RRA ratios (X_1) and temperatures (X_2) on the synthesis process. Table 1 provides the five levels of experimental variables which were derived from CCD. To make the model, 17 experiments were carried out including 9 replications at the center points. The coded values of the parameters employed for design were computed using Eq. (1):

$$X_i = \frac{(X_0 - X_1)}{\Delta X} \quad (1)$$

where X_i refers to the value of a dimensionless coded variable. $X_0$is the uncodedvariable at the center point and X_1representsthe value of and the value of the uncoded variable, ΔX is the step change value.

The experimental results that were analyzed by the specific surface area of the synthesized adsorbent at different situations were computed using the second-order polynomial model (quadratic model) as illustrated in Eq. (2):

$$Y = B0 + \sum_{i=1}^{k} X_i B_i + \sum_{i=1}^{k} X_i^2 B_{ii}^2 + \sum_{i=1}^{k-1} \sum_{j=2}^{k} X_i X_j B_{ij} + C \quad (2)$$

where Y represents the output response (SSA based on m^2/g), B_0 is a constant value, and B_i, $B_{ii,}$ and B_{ij} refer to the regression coefficients for linear, second-order and interactive effects, respectively, X_i and X_j are independent factors and C represent the error of prediction. DESIGN EXPERT, version 7.0.0 was used to analyze the results [32]. Then, the optimal condition for the adsorbent production was calculated through the Solver "add-in" application in Microsoft Excel.

Based on the model, RRA was mixed with different KOH/RRA ratios for 1 day in 0.1 L of deionized water. The product of this stage was denoted as KRA. The product was filtered, and then washed with distilled water until reach solution pH to a neutral state. Finally, the KRA was further regenerated using the carbonization process. According to the suggested temperatures of the RSM method, KRA was carbonized in the presence of nitrogen gas flow (5 L/min) in an electric furnace for 2 h.

Modification of GGN to anionic green-graphene nanosheet (MAGGN) using a grafting amine group method

The surface modification of GGN was carried out for achieving the highest ion exchange capacity with a grafting amine group based on previous study results [33].

The following procedure was used for cross linking of GGN with epichlorohydrin; 75 mL of N, N-dimethylformamide and 76 mL of triethylamine was increased to a9mL aliquot of epichlorohydrin. Then, the mixture was mixed for 2 h at 80 °C. Next, 10 g of GGN was increasedto50mL of the mixture in a flask with 250 mL. Finally, pyridine (10 mL) was aggravated to the well-mixed solution and blended for 2 h at 60 °C. The precipitate was separated with paper filter and washed repeatedly with one liter of HCl and (0.1 M) NaOH (0.1 M) and then widely rinsed with distilled water. The final product was called anionic green graphene nanosheet (AGGN). These products were dried using a vacuum method, subsequently sieved to reach the particle size of 149 μm and kept at laboratory conditions.

Characterization of the adsorbent

N_2 molecule adsorption-desorption was carried out using a BELSORP-mini-II (BEL Japan, Inc.) at 77 K to calculate the specific surface area (SSA) of adsorbents from various KOH/RRA ratios and temperatures and the optimization of GGN production [34]. The SSA was computed by the Brunauer, Emmett, and Teller (BET) equation [35]. For determining the characterization and mineral identification of the samples (RRA, KRA, and GGN), the XRD analysis was performed using X-ray diffractometer (Shimadzu, model: XD-5A) with a source of Cu Kα (λ = 1.541 Å) [36]. Fourier transform infrared (FT-IR) spectra were measured with Fourier Transform Infrared (model: EQUINOX 55, Germany) and RAMAN spectra of the samples were determined with a spectrometer of an Almega spectrometer of Thermo Nicolet Dispersive Raman, respectively [37]. Transmission electron microscope (TEM) was used for determining the morphology of GGN at 100 kV [38].

Table 1 Experimental ranges and levels of independent variables used in CCD design for the production of Green-Graphene nanosheet

Original Independent Variables	Unit	Coded symbol	Coded levels of variables				
			-α	-1	0	+1	+α
KOH/RRA	–	X_1	8	8.63	10	11.37	12
Temperature	°C	X_2	500	562.74	700	837.26	900

Chromium solution and analytical method

As described in Standard Methods [39], a stocksource aqueous solution of Cr (VI) was provided with141.4 mg of potassium dichromate in distilled water (100 mL).The desired Cr(VI) concentration was obtained through dilution of the stock solution with deionized water [40]. The UV–Vis Spectrophotometer (HACH DR-5000, USA) was used for determining the Cr (VI) concentration at λ_{max} value of 540 nm. The desired solution pH was obtained using HCl (0.1 N) and NaOH (0.1 N).A Metrohm pH meter (827-pH lab, Switzerland) was employed to analyze the pH values.

Adsorption tests

Adsorption experiments were performed as a batch reactor in a vial of 40 mL. In each run of experiments, 30 mL of the contaminated water was transferred to each vial, an exact value of adsorbent was increased to the solution, and the suspension was agitated at 200 rpm at the anticipated time. Finally, the supernatant of samples was separated for 10 min with the centrifuge device at 18,000 rpm and the residual of hexavalent chromium was measured. The adsorption capacity and removal efficiency of hexavalent chromium were determined according to eqs. (3) and (4), respectively:

$$q = \frac{(C_{in} - C_t) \times V}{W} \tag{3}$$

$$E = \frac{(C_{in} - C_t) \times 100}{C_{in}} \tag{4}$$

WhereE is the removal efficiency of hexavalent chromium (%), C_{in} and C_t represent the initial concentration of hexavalent chromium Cr (VI) (mg/L) and the concentration of hexavalent chromium at time of t after the adsorption process (mg/L), V, W and q refer to the Cr (VI) adsorption capacity (mg/g), solution volume (L) and dose of adsorbent (g), respectively.

Experiment design for adsorption tests

A five-level four-factor CCD approach was employed to evaluate the effective factors on the hexavalent chromium removal. The RSM was applied to specify the interaction independent variables effects which include contact time (min), hexavalent chromium concentration (mg/L), adsorbent concentration (g/L), and solution pH. The independent variable levels at CCD for chromium (IV) removal are presented in Table 2.The coded value used for the variables was calculated using eq. (1). Eq. (2) was applied to determine the interaction between the hexavalent chromium removal efficiency (response) and independent variables. The optimization of results of the analysis of variance (ANOVA) model predicted through experimental design was in the Microsoft Excel Solver "add-in".

Results and discussion

Characterization of green-graphene nanosheet

RSM model analysis for production of green-Graphene nanosheet

Table 3 presents all observed, predicted, and residual values along with experimental conditions using the quadratic model. Also, the variance analysis (ANOVA) results for the specific surface area of Green-Graphene nanosheet is shown in Table 4.

As revealed in Table 4, the adjusted correlation coefficient ($R^2 = 97.44$) was in reasonable agreement with the multiple R^2 (98.30) and these values indicated that the quadratic model can sufficiently predict the impact of independent variables (KOH and temperature) on the response (SSA of GGN). The non-significant Lack of Fit (0.1363) and significant *p* value (<0.05) confirmed that the response surface quadratic model is significant and coulddescribeas well the GGN synthesis process.The F-Value and p value define the importance and significance of each coefficient. Based on the coefficient results, the effect of KOH treatment was more significant than the carbonization temperature. Therefore, increasing the SSA level of raw rice ash from 40to about 550 m^2/g affected by the KOH treatment more thanthe carbonization temperature.

The optimal condition of the GGN synthesis process was obtained using the Solver "add-in" and additional laboratory experiments were done to confirm the validity of the quadratic model. The optimum synthesis conditions predicted by RSM were a KOH/RRA ratio of 10.85, a temperature of 749.61 °C, and the maximum SSA of GGN was estimated to be 547.75 m^2/g. Based on the three additional laboratory experiments at optimum conditions, the obtained SSA was 551.14 ± 3.83 m^2/g. SSA of rice straw (<149 μm), RRA, KRA, and GGN were 0.73, 40.62, 359.36, and 547.75m^2/g, respectively. Therefore, the TCR method caused the SSA to increase, while, the oxidation of agricultural waste alone usually causes a substantial decrease in SSA [41].

A contour plot which represents the simultaneous effects of variables on the GGN synthesis is depicted in Fig. 1.The results represented thatthe lower active surface of the final product isachieved with increasingthe synthesis temperature of GGN to more than 750 °C.

Patterns of X-ray diffraction (XRD) of RRA, KRA, and GGN

Figure 2 displays XRD patterns of RRA, KRA, and GGN. The XRD pattern of RRA showed numerous peaks but the

Table 2 Experimental ranges and levels of independent variables used in CCD design for Cr (VI) adsorption experiments

Original independent variables	Unit	Coded symbol	Coded levels of variables				
			-α	-1	0	+1	+α
pH	–	X_1	4	5.69	7	8.31	10
Time	min	X_2	10	24.11	35	45.89	60
Adsorbent	g/L	X_3	0.1	0.64	1.46	1.49	2
Cr (VI)	mg/L	X_4	10	35.39	55	74.60	100

main two-theta angle peakswere22°, 27°, 29°, and 41°.The peak appearing at 2θ = 26° could be attributed to the main index of graphite representing an interlayer space of about 3.34 Å. The graphitic peak and peaks related to other impurities disappeared after the treatment with KOH. At this stage, KOH treatment has a dual function: removing the impurities, especially silica (at around 2θ = 23°) and increasing the distance between graphitic sheets by KOH penetration into the interlayer space of the basal plane.

In the second stage (carbonization), the reduction process was completed and low intensity of broad peak appeared at around two-theta angles of 25° belonging to the sheets of graphene and no graphitic peak was observed in the XRD pattern of GGN at 750 °C. The XRD peak of GGN was similar to typically reduced graphene oxide XRD patterns that were reported in the literature [20, 42, 43].

In addition, the XRD pattern of GGN at 900 °C (Fig. 2d) confirms that temperature over the optimal level (750 °C) could result in agglomeration or rearrangement of the graphene plates and reoccurrence of the graphitic peak. Comparing the results of experimental design with XRD pattern results shows that increasing temperature to more than the optimum could lead to a decreased active surface of synthesized graphene perhaps due to the agglomeration of graphene surfaces. Therefore, the carbonization temperature applied to the synthesis of graphene should be carefully controlled to be less than 800 °C.

RAMAN spectroscopy analysis of RRA, KRA, and GGN

A Raman spectrometer was used to monitor the change in the geometric structure of the adsorbent during the synthesis process. The RAMAN spectrum of the RRA, KRA, and GGN are shown in Fig. 3. The sharp peak appearing at about 1330 cm^{-1} represents a D band at the graphene sheets edge plane that is related to amorphous carbon [44]. In addition, to remove the impurities and increase the ability of penetration, KOH can efficiently be used to remove amorphous carbon [21].

Table 3 Observed, predicted and residual values for the specific surface area of Green-Graphene nanosheet

Run No.	Actual variables		Observed SSA (m^2/g)	Predicted SSA (m^2/g)	Residual SSA (m^2/g)
	KOH	Temp			
1	8.627	562.740	290.936	302.523	−11.587
2	11.373	837.260	540.745	524.887	15.858
3	10	700	540.774	515.276	25.498
4	10	700	525.656	515.276	10.380
5	8.627	837.260	341.463	330.235	11.228
6	10	700	514.579	515.276	−0.697
7	10	700	500.507	515.276	−14.769
8	10	700	523.954	515.276	8.678
9	11.373	562.740	390.949	397.906	−6.957
10	10	700	525.740	515.276	10.464
11	10	700	516.440	515.276	1.164
12	10	900	415.199	433.147	−17.948
13	10	700	505.424	515.276	−9.852
14	12	700	485.604	491.072	−5.468
15	10	500	333.814	320.447	13.367
16	8	700	280.654	279.767	0.887
17	10	700	499.456	515.276	−15.820

Table 4 Analysis of variance (ANOVA) for the specific surface area of Green-Graphene nanosheet

Source	Sum of Squares	df	Mean Square	F Value	p valueProb > F
Block	5257.166	1	5257.166		
Model	127,422	5	25,484.39	115.3954	< 0.0001
A-KOH	43,355.01	1	43,355.01	196.315	< 0.0001
B-TEMP	12,333.19	1	12,333.19	55.84571	< 0.0001
AB	2463.584	1	2463.584	11.15531	0.0075
A^2	33,054.61	1	33,054.61	149.674	< 0.0001
B^2	37,589.96	1	37,589.96	170.2104	< 0.0001
Residual	2208.44	10	220.844		
Lack of Fit	1159.408	3	386.4692	2.578837	0.1363
Pure Error	1049.033	7	149.8618		
Cor Total	134,887.6	16			

Multiple R^2 = 0.9830, Adjusted R^2 = 0.9744, Std. Dev. = 14.86, Mean = 454.82, C.V. % = 3.27, Pred R-Squared = 0.9009, PRESS = 12,843.62, Adeq Precision = 26.713

Therefore, it could be cleared in Fig. 3(b) that the chemical treatment by KOH had a significant impact on the D band of the spectrum of adsorbent (KRA). So, the GGN was amorphous carbon-free and had clean edges.

The second band appearing around 1583 $cm^{-1}$was the band of G that included the graphene sheets. Since the band of G is extremely sensitive to the graphene layers number, its intensity and frequency arevery important to estimate the impact of each synthesis stage of the GGN production. By reducing the graphene layers number, the G band intensity was reduced. As shown in Fig. 3, with the progress in the production process from RRA to KRA and GGN, the intensity of the Raman shift declined from 3139 to 2969 and 2397, respectively. In addition, by decreasing the graphene layers number, the G band shifts to a higher wave number. The variations in intensity and frequency of the G band represent suitable delamination of the graphene sheets and formation of low-layer graphene.

On the other hand, graphene can be detected by analyzing the intensity ratio of the G to the D band (I_G/I_D), since it represents the amount of uniformity in the structure of graphene [45]. According to the Raman spectrometer results, the I_G/I_D ratios for RRA, KRA, and GGN were equal to 0.675, 0.767, and 0.777, respectively. Therefore, the TCR process by KOH and temperature resulted in the effective removal of amorphous carbon and production of the GGN with clean edges. The I_G/I_D ratio of GGN was similar to the typically reduced graphene oxide that was previously found [46].

FT-IR spectroscopy analysis of RRA, KRA, and GGN in comparison with zero-point charge (pHzpc)

The removal of functional groups containsoxygen during the RRA reduction was investigated by FT-IR spectroscopy (Fig. 4). As shown in Fig. 4 (a), the presence of different functional

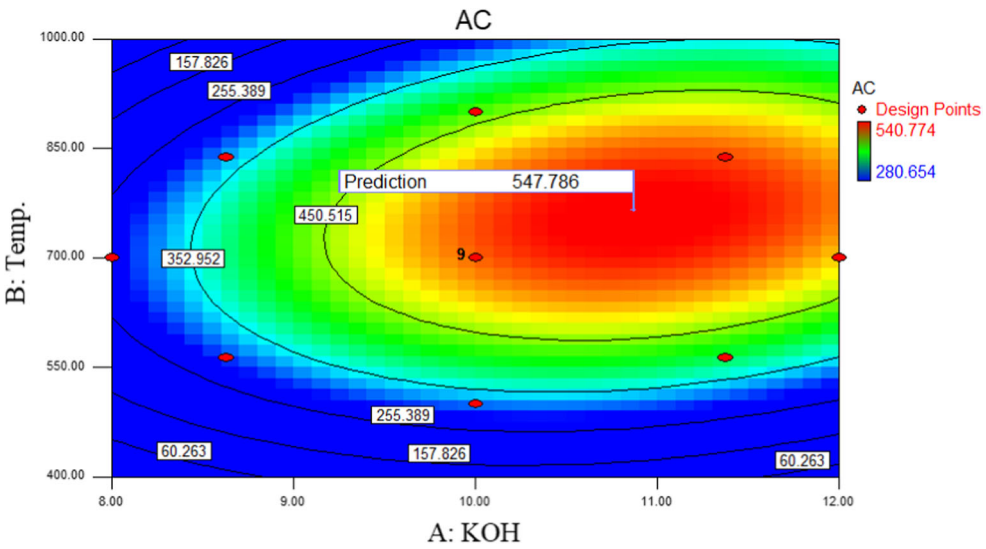

Fig. 1 Contour plot of the variable's effects on the GGN surface area

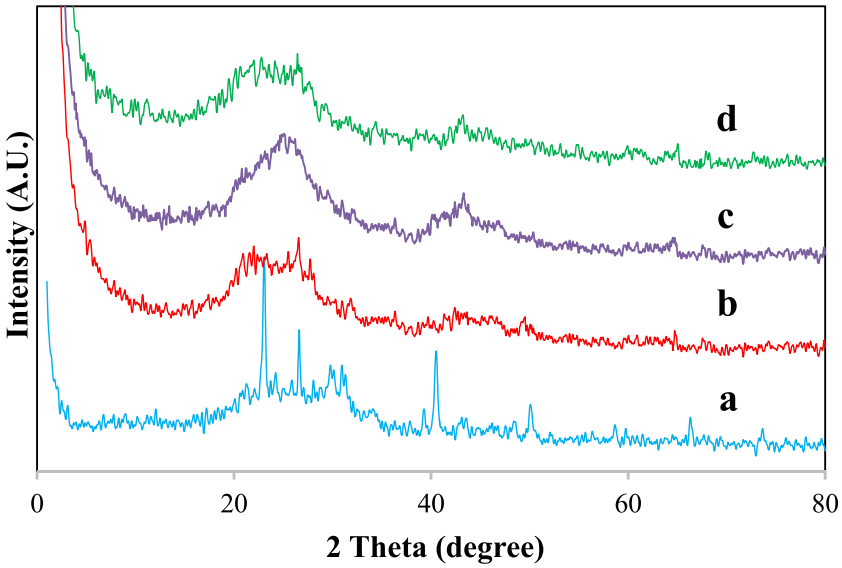

Fig. 2 The XRD patterns of (**a**) RRA combusted at 280 °C (**b**) KRA with KOH/RRA ratio of 10.85 (**c**) GGN at 750 °C and (**d**) GGN at 900 °C

groups including C–O (1077 cm^{-1}), OH (3280 cm^{-1}), and C–OH (1340 cm^{-1}), indicates that oxygen-containing groups were present in RRA. But, the main FT-IR peaks of rGO appear from 3200 to 3700 cm^{-1} and 1600 to 1650 cm^{-1} belonging to the hydroxyl and alkenyl functional groups, respectively [20, 44]. As shown in Fig. 4(c), the oxygen-containing functional groups obviously decreased due to reduction phenomenon, and the peak of hydroxyl and alkenyl groups remained. Therefore, the FT-IR image completely confirmed the reduction of RRA to graphene. On the other hand, Infrared spectra could present the structure changes for adsorbents which contain different functional groups. Thus, IR spectra were employed to confirm the conversion of GGN to MAGGN using grafting amine group as a weak basic ion exchanger (Fig. 4 (d)).

As shown in Fig. 4 (c and d), there is a similarity in the fingerprint region (a wavelength of less than 1000 or 1200 cm^{-1}) indicating a similarity of the original GGN structure and the MAGGN. However, in the functional group region, significant changes have been made after the association of amine groups on the GGN surface. As expected, the radiation intensity of the hydroxyl group at 3431 cm^{-1} increased from 3.604 to 18.918%. The reason for this phenomenon is that the anionic exchange resin has a lower adsorption rate in the wavelengthrange of 3200 to 3600 cm^{-1} [47].Also, the peak perceived at 1367 cm^{-1} is related to the tensile vibrations caused by the C-N bond which confirms that amine groups are located on the MAGGN. Results indicate that there is a weak peak at a wavelength of 1411 cm^{-1}because of deformed vibrations

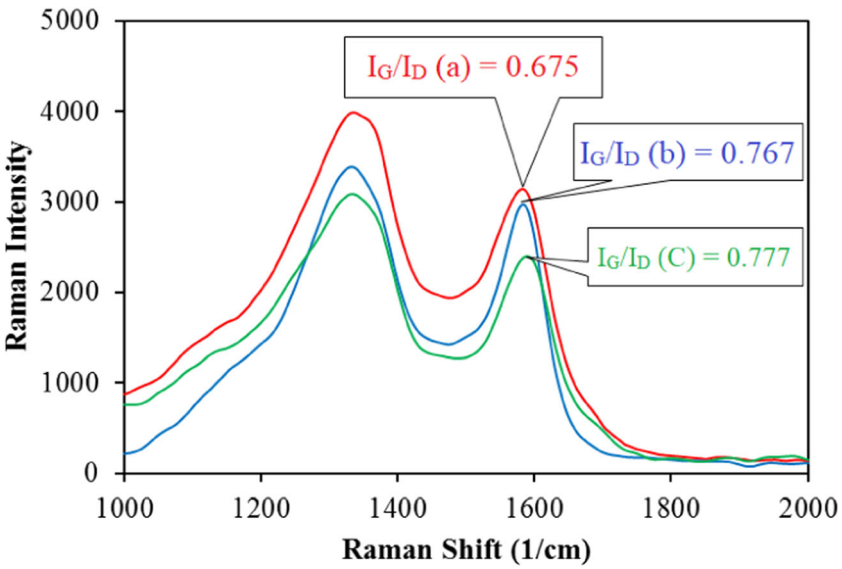

Fig. 3 The RAMAN spectra of (**a**) RRA combusted at 280 °C (**b**) KRA with KOH/RRA ratio of 10.85 and (**c**) GGN at 750 °C

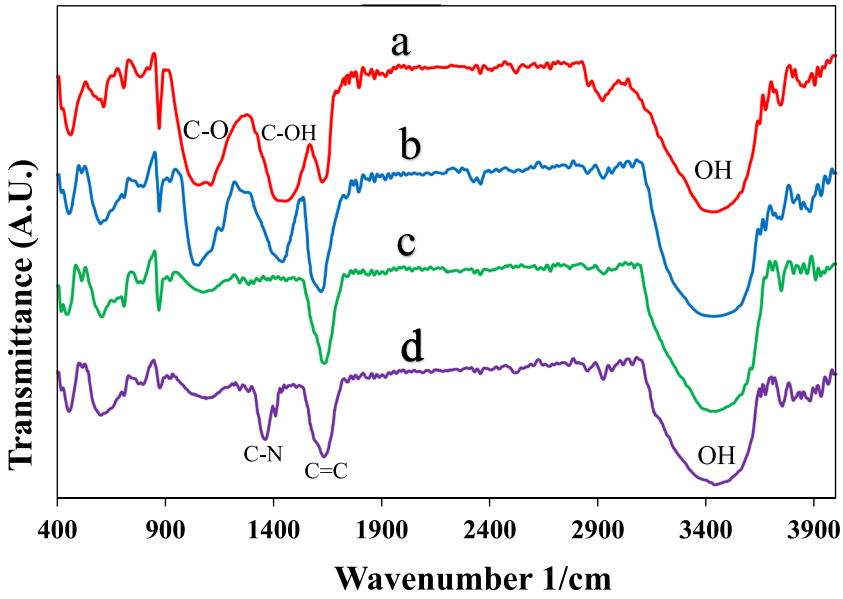

Fig. 4 FTIR spectrumof (**a**) RRA combusted at 280 °C (**b**) KRA with KOH/RRA ratio of 10.85 (**c**) GGN at 750 °Cand (**d**) modified GGN using grafting amine group method

of -NH, but the strong peak of 1367 cm^{-1}shows that many amine groups have been linked to the MAGGN surface.

In another study, Katal et al. 2012, studied rice bran for the synthesis of ion exchange resins to remove nitrate. They reported that amine groups have appeared in wavenumber of 1360 cm^{-1}. Also, the addition of amine groups on the surface of the adsorbent increased zeta potential from −33 mV to +38 mV, which had a meaningful impact on increasing the adsorption capacity of anions [48].

According to the results, the pH of the zero-point charge of GGN was 4.1. Generally, the pHzpc of graphene depends on the synthesis method and the graphene layer number established on the surface of the adsorbent. For instance, Zhao et al. 2011found the pHzpc of low-layer graphene was 3.9 [49], while Song et al. determined the pHzpc to be 5.35 [50]. Konkena et al. reported a value of 4 for pHzpc, which is similar to the result of this study [51]. Usually, the pHzpc of graphene has been reported in a rangeof 3.5 to 5.5 [52].

Therefore, it can be expected that adsorption of anions on the synthesized graphene occurs at acidic pH (less than 4). However, graphene surface modification and changes in the functional groups can affect the pHzpc of graphene, thereby improving the adsorption efficiency. Results indicated that the pHzpc of MAGGN was 7.9 which was in favor of higher adsorption capacity for anions. In fact, the bonding of amine groups increased the zeta potential and these phenomena led to improved adsorption of anionic compounds. The results of infrared spectrum analysis and pHzpc measurements both confirmed the amine group's presence as an active function on the surface of MAGGN.

Image of transmission Electron microscopy (TEM) of GGN

The TEM image of GGN is represented in Fig. 5. The dark and light color of graphene edges in the TEM image illustrates the number of layers on the surface of the synthesized sample. In addition, graphene is classified with the associated number of layers. The graphene with 3 to 10 layers is classified as few-layer graphene and 10 to 30 layers as thick graphene or a graphite thin nano-crystal. Therefore, the synthesized graphene could be considered as two-layer graphene or few-layer graphene. Furthermore, the TEM images indicated that synthesized graphene had soft and clean edges.

Analysis of the RSM model for Cr (VI) removal

Table 5 illustrates the experimentaldesign, observed, predicted, and residual values for removal efficiencies (%) of hexavalent chromium by applying a quadratic model. The statistical significance of models that represents the variance

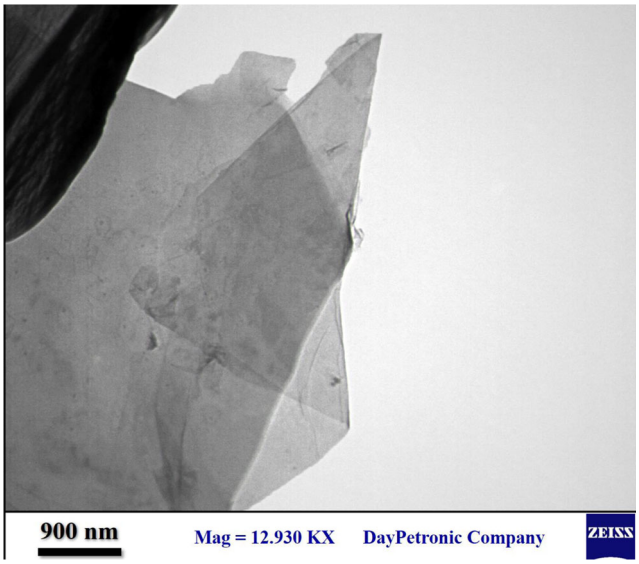

Fig. 5 The TEM image of GGN obtained from thermo-chemical reduction process

analysis (ANOVA) for the hexavalent chromium removal from polluted water is shown in Table 6.

As revealed in Table 6, the adjusted R^2 (94.59) was close to the multiple R^2 (96.39). Thus, the response surface quadratic model might accurately predict the alteration of independent variables on the hexavalent chromium removal from aqueous solution. The significant p value (<0.05) and non-significant Lack of Fit (0.0694) showed that the model of the quadratic was sufficiently significant and can efficiently predict the Cr (VI) removal.

The results showed that all variables had significant effect on the Cr (VI) removal, but the interaction between reaction time and pH ($X_1 \times X_2$), Cr (VI) concentration and pH ($X_1 \times X_4$), and the amount of adsorbent and time of the reaction ($X_2 \times X_3$) was non-significant and had a p value less than 0.05. Also, F-values revealed that the adsorbent dose was the most effective parameter on the Cr (VI) removal (highest F-value). The adsorption sites may increase with adsorbent dose and the resistance of mass transfer between the adsorbent and adsorbate decrease with more adsorption sites [53].

A quadratic regression equation (Eq. (5)) for the hexavalent chromium removal was developed by applying multiple regression analysis in terms of actual factors as follows:

$$\begin{aligned} Cr\ (VI)\ removal\ efficiency\ (\%) = {} & -191.397 + 50.58799*pH \\ & + 1.399904*Time + 131.783*Ads - 0.45364*Cr \\ & - 4.37016*pH*Ads + 0.012706*Time*Cr \\ & + 0.253045*Ads*Cr - 3.30947*pH^2 - 0.01816*Time^2 \\ & - 35.3905*Ads^2 - 0.0073*Cr^2 \end{aligned} \quad (5)$$

Table 5 Observed and predicted values for Cr (VI) removal from contaminated water

Run No.	Observed values (%)	Predicted values (%)	Residual	Run No.	Observed values (%)	Predicted values (%)	Residual
1	79.78	88.55	8.77	23	70.60	73.72	3.12
2	57.49	59.45	1.95	24	71.79	64.40	−7.39
3	89.45	89.51	0.06	25	70.80	67.74	−3.05
4	88.44	88.55	0.11	26	86.69	88.55	1.86
5	91.51	88.55	−2.96	27	86.67	88.55	1.88
6	85.77	88.55	2.78	28	68.53	65.87	−2.65
7	86.47	86.00	−0.47	29	91.09	87.93	−3.16
8	76.13	74.03	−2.10	30	88.46	88.55	0.09
9	91.60	88.55	−3.05	31	56.91	55.13	−1.78
10	86.72	88.40	1.68	32	89.74	87.36	−2.39
11	86.80	89.03	2.23	33	62.14	64.20	2.06
12	41.09	35.87	−5.22	34	85.38	88.55	3.17
13	73.16	73.67	0.52	35	86.08	88.55	2.48
14	91.67	88.55	−3.12	36	59.46	62.40	2.94
15	90.99	88.48	−2.50	37	22.32	25.86	3.54
16	89.97	88.55	−1.42	38	55.29	59.60	4.32
17	46.40	45.69	−0.71	39	94.84	88.55	−6.29
18	50.92	55.02	4.11	40	91.11	90.20	−0.91
19	89.63	88.55	−1.08	41	86.97	88.55	1.58
20	87.26	88.55	1.29	42	88.72	88.55	−0.17
21	88.64	92.99	4.34	43	91.07	88.55	−2.52
22	87.44	88.55	1.11	44	91.57	88.55	−3.02

Table 6 Analysis of variance (ANOVA) for Cr (VI) removal from contaminated water

Source	Sum of Squares	df	Mean Square	F Value	p value Prob > F
Block	21.19979	1	21.19979		
Model	11,484.83	14	820.3447	53.41542	< 0.0001
A-pH	66.64823	1	66.64823	4.339692	0.0465
B-Time	851.6106	1	851.6106	55.45125	< 0.0001
C-Ads	4762.527	1	4762.527	310.1042	< 0.0001
D-Cr (VI)	1010.612	1	1010.612	65.80435	< 0.0001
AB	0.198576	1	0.198576	0.01293	0.9103
AC	89.48727	1	89.48727	5.826819	0.0226
AD	11.50603	1	11.50603	0.749196	0.3941
BC	18.85482	1	18.85482	1.227701	0.2773
BD	117.8665	1	117.8665	7.674687	0.0098
CD	67.50643	1	67.50643	4.395572	0.0452
A^2	1771.856	1	1771.856	115.3715	< 0.0001
B^2	257.2699	1	257.2699	16.75172	0.0003
C^2	2037.481	1	2037.481	132.6673	< 0.0001
D^2	436.519	1	436.519	28.42323	< 0.0001
Residual	430.0191	28	15.35783		
Lack of Fit	236.6911	10	23.66911	2.203737	0.0694
Pure Error	193.328	18	10.74044		
Cor Total	11,936.045	43			

Multiple R^2 = 0.9639, Adjusted R^2 = 0.9459, Std. Dev. = 3.92, Mean = 78.49, C.V. % = 4.99, Pred R-Squared = 0.8546, PRESS = 1732.22, Adeq Precision = 28.401

The optimal conditions resulting from the Solver "add-in" for Cr (VI) removal from contaminated water (98.57%) were: adsorbent dose: 1.46 g/L,pH: 6.87, reaction time: 44.30 min, and Cr (VI) concentration: 48.35 mg/L. The result of the hexavalent chromium removal efficiency at the optimum condition from the contaminated water was 96.35% ± 1.85. In addition, the optimum conditions were appliedfor the hexavalent chromium removal from real contaminated wastewater samples. The results of Cr (VI) removalat the optimum conditionsindicatedthe removal efficiency of 89.66% ± 2.92. The slight (6.5%) decline in the removal efficiency was because ofthe existence of high dissolved solids inthe real Cr (VI) wastewater. Therefore, GGN could be considered as an efficient adsorbent for treating the contaminated wastewater.

Contour plots which could simultaneously reflex the effects of interaction between the variables on the removal of Cr (VI) are depicted in Fig. 6. The effects of solution pH (X_1) and contact time (X_2) on the Cr (VI) removal are shown in Fig. 6a. The GGN dose and initial hexavalent chromium concentration were 1.44 g/L and 56.61 mg/L, respectively. According to Fig. 6a, most of Cr (VI) removal efficiency (about 90%) were obtained at less than 30 min. The high rate of adsorbed Cr (VI) could be associated with the high attraction of adsorbate to the functional groups of hydroxyl on the GGN surface [54].

The high amount of the estimated coefficient for (X_1) shows that pH had a vital role in the adsorption of hexavalent chromium due to its impact on the functional groups located on the adsorption surface. As observed in Fig. 6a, the maximum removal of hexavalent chromium occurred at a natural pH. This is attributed to the competition between Cr (VI) and OH- for adsorbing on the adsorbent surface and a greater amount of surface functional groups [33].

The pH effects (X_1) and GGN dosage (X_3) on the removal of hexavalent chromium can be seenin Fig. 6b. In this step, the initial concentration of Cr (VI) and contact time were 56.61 mg/Land 43.80 min, respectively.It is comprehended from Fig. 6b that the removal ofCr (VI) was very sensitive to variations of the GGN dosage at low and high pH. The main reason for enhancement in the Cr (VI) removal efficiency with increasing GGN dosage could be because ofthe enlargement in the free available adsorption sites [55, 56].

The effects of the concentrationof hexavalent chromium(X_4) and GGN dosage (X_3) on the hexavalent chromiumadsorption are illustrated in Fig. 6c. In addition, the contact time and pH were 43.80 min and 6.23, respectively. The effect of adsorbate concentration on the removal efficiency of hexavalent chromium was reverse. Thus, the highest removal of hexavalent chromium occurred at the lowest concentration because of sufficientfree available adsorption sites at a hexavalent chromium low concentration [57].

Adsorption isotherm and kinetic studies

In this work, the most common adsorption isotherm [36, 58] (Langmuir,Freundlich, and Temkin) were studied for analyzing the data obtained from adsorption of hexavalent chromium (from contaminated water solutions) on the GGN after 24 h mixing. The linear equation, variables,and values of isotherms are shown in Table 7.

According to the results, the results of Cr (VI) adsorption onto GGN was well fitted withLangmuir isotherm (R^2 = 0.991). Figure 7 shows the isotherm models of Langmuir, Freundlich, and Temkin. The Langmuir isotherm model describes the kinetic principles and monolayer coating of the Cr (VI) (adsorbate) onto the GGN (adsorbent) surface. According to the Langmuir assumptions, the adsorption process takes place on the homogenous surface with definite adsorption sites (with functional group of hydroxyl) where they have the equalenergy of adsorption. Themaximum capacity of adsorption (q_m) for Cr (VI) by GGN was 138.89 mg/gaccording to the Langmuir model. This suggests that the adsorption capacity of GGN was higher than those found by studies conducted on the carbon nanotubes [59], tea waste/Fe3O4

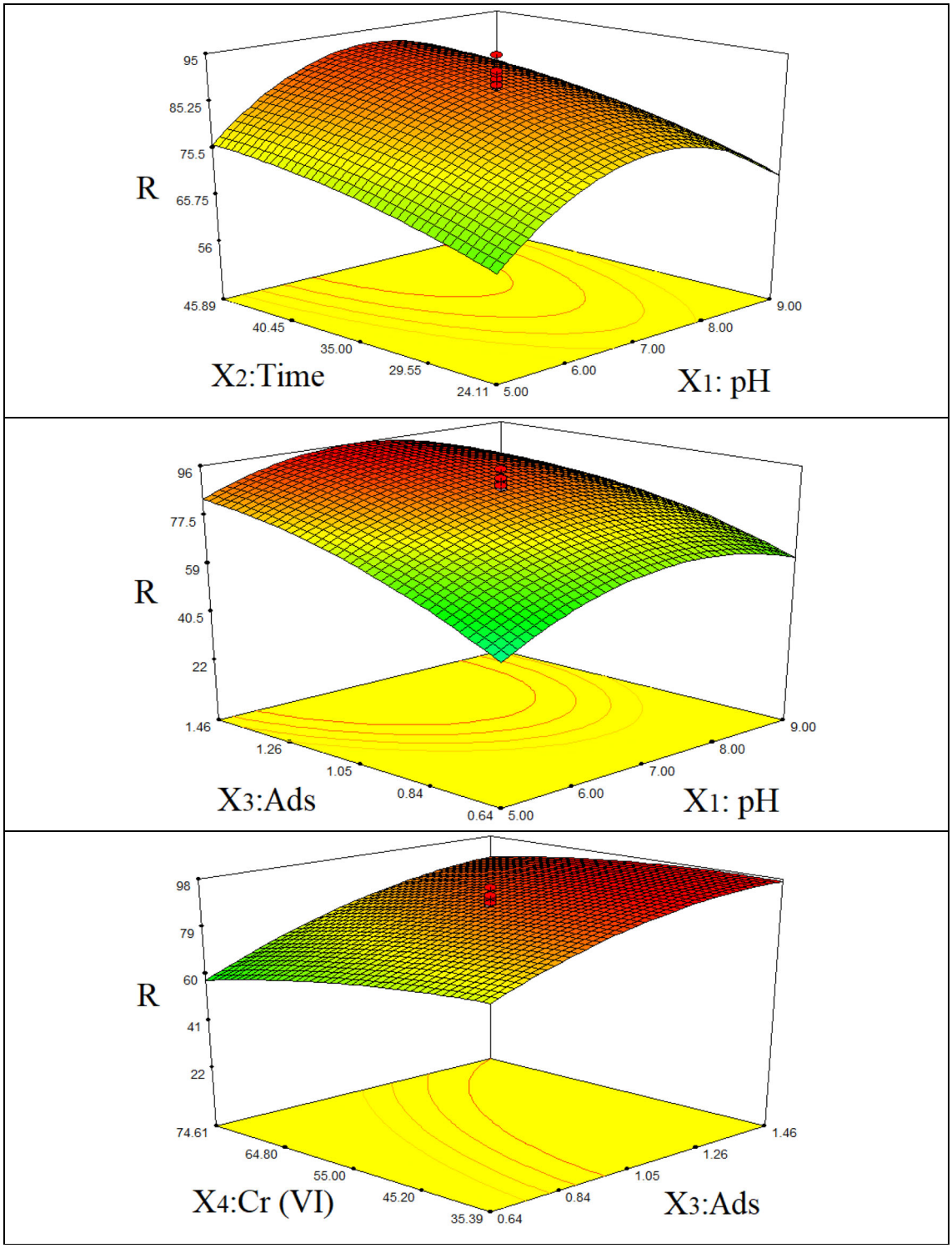

Fig. 6 Contour plots for the interaction effect of variables on the Cr (VI) removal. (**a**) contact time (min) and pH, (**b**) adsorbent dose (g/L) and pH, and (**c**) Cr (VI) concentration (mg/L) and adsorbent dose (g/L)

nanoparticle [3], magnetic nanocarbon [1], bamboo-like polypyrrole nanofibrous mats [8], and Chitosan/Polyvinyl alcohol/Zeolite Composite [4] as an Cr (VI) adsorbate.

The most common kinetic models [60, 61] (pseudo-first and second-order; Elovich and Intraparticle Diffusion model) were selected to evaluate the reaction rate of the removal of Cr (VI) through the GGN. The linear equations and characteristics of kinetic models are listed in Table 8. The kinetic study was performed at a contact time of 1 to 24 h. According to the results (Fig. 8), the pseudo-second-

Table 7 Isotherms and their parameters for Cr (VI) removal from contaminated water

Isotherm	Linear equation	Plot	Parameters	values
Langmuir	$\frac{C_e}{q_e} = \left(\frac{1}{K_L q_m}\right) + \left(\frac{1}{q_m}\right) C_e$	C_e/q_e vs. C_e	R^2	0.991
			q_m (mg/g)	138.89
			K_L (L/mg)	0.223
Freundlich	$\log(qe) = \log(K_f) + \left({}^1/_n\right)\log(C_e)$	log (q_e) vs. log (C_e)	$R^2 n_F$	0.965
			K_F (mg/g)	3.662
				5.129
Temkin	$q_e = B_T \ln A_T + B_T \ln Ce$	q_e vs. ln (C_e)	R^2	0.9
			A_T (L/mg)	2.683
			B_T (J/mol)	28.336

orderrepresent more appropriate conditions to predict the reaction rate of Cr (VI) adsorption on the GGN (R^2 = 0.999).

Conclusion

Chromium (VI) removal was successfully carried out using the Green-graphene nanosheet (GGN) prepared from agricultural waste. The prepared GGN at optimum conditions showed a good specific surface area (550 m^2/g), close to 650 and 14 times higher than the rice straw and rice straw ash, respectively. However, synthesis temperatures higher than the optimal level (750 °C) led to reduced SSA of the GGN; therefore, the carbonization temperature should be carefully controlled. The removal efficiency of hexavalent chromium was enlarged with the adsorbent amount and contact time. The removal of hexavalent chromium also declined at the high initial concentration of hexavalent chromium. In addition, the maximum percentage removal of hexavalent chromium

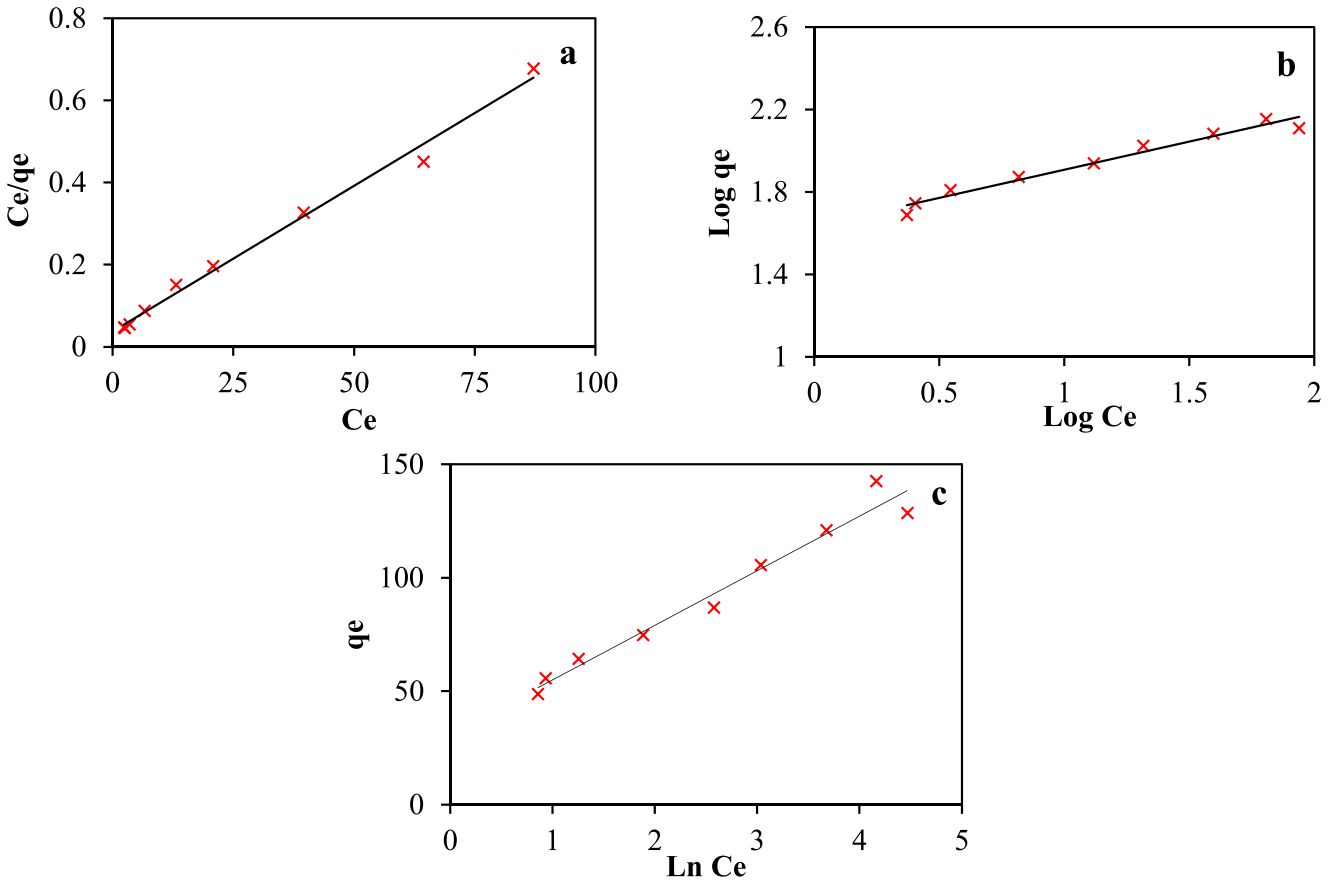

Fig. 7 Application of (**a**) Langmuir, (**b**) Freundlich, and (**c**) Temkin isotherm models to Cr (VI) adsorption onto GGN

Table 8 Kinetics and their parameters for Cr (VI) removal from contaminated water

Kinetic model	Linear equation	Plot	Parameters	values
Pseudo first-order	$\log(q_e - q_t) = \log(q_e) - \frac{k_1}{2.303}t$	$\log(qe - qt)$ vs. t	R^2	0.702
			q_e (mg/g)	2.898
			k_1 (1/min)	0.001
Pseudo second-order	$\frac{t}{q_t} = \left(\frac{1}{k_2 q_e^2}\right) + \left(\frac{1}{q_e}\right)t$	t/qtvs. t	R^2	0.999
			q_e (mg/g)	68.493
			k_2(g/(mg.min))	0.005
Elovich	$q_e = \left(\frac{1}{\beta}\right)\ln(\alpha\beta) + \left(\frac{1}{\beta}\right)\ln t$	qt vs. $\ln(t)$	R^2	0.958
			β (g/mg)	0.097
			α(mg/(g.min))	131.512
Intraparticle Diffusion	$q_t = K_{dif}t^{0.5} + C$	q_t vs.$\sqrt{t}$	R^2	0.841
			C (mg/g)	31.069
			K_{dif} (mg/(g.min$^{0.5}$))	5.137

occurs at natural pH value. According to the Langmuir equation, the highest chromium monolayer capacity of adsorption of GGN was 138.89 mg/g. The experimental data was the best fit with the kinetic equation of pseudo-second-order. Using rice straw as a starting material, not only could minimize the disposal problem, but also an agricultural waste can be transformed into a valuable adsorbent material. In conclusion, modified rice straw-based Green-Graphene Nanosheet (GGN) could be employed as a favorable and fast adsorbent for the separation of hexavalent chromium from aqueous environments and even real wastewaters contain hexavalent chromium.

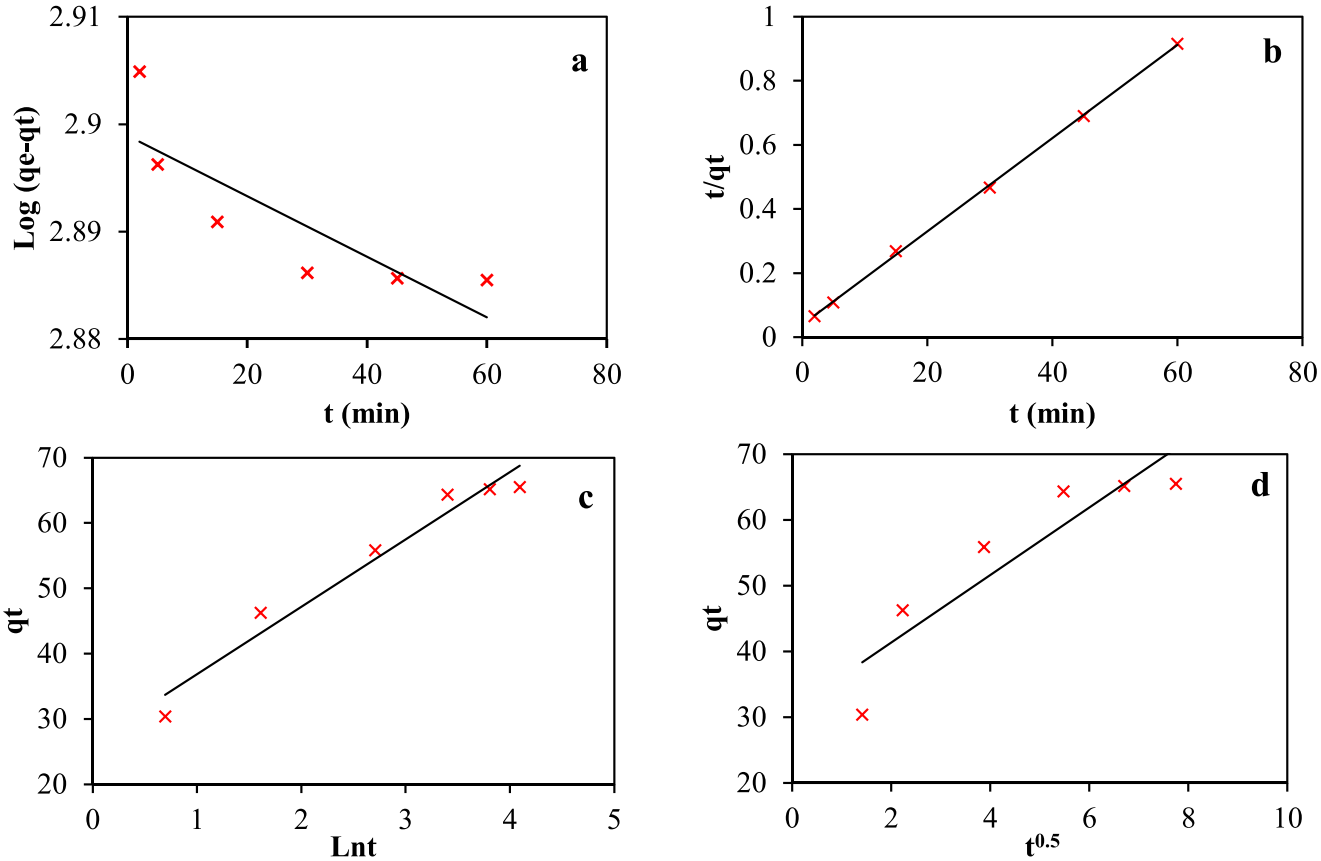

Fig. 8 Application of (**a**) pseudo-first-order, (**b**) pseudo-second-order, (**c**) Elovich and (**d**) intraparticle diffusion kinetic models to Cr (VI) adsorption onto GGN

Acknowledgments This research has been financially supported by Shahroud University of Medical Sciences, Shahroud, Iran with a grant (Project No: 96132) and registered in Ethics Committee under ID no: IR.SHMU.REC.1396.131. The authors would like to appreciate the technical collaborations of the Department of Environmental Health Engineering, School of Public Health, Shahroud University of Medical Sciences.

Compliance with ethical standards

Conflict of interest The authors declare that they have no conflict of interest.

References

1. Huang J, Cao Y, Shao Q, Peng X, Guo Z. Magnetic nanocarbon adsorbents with enhanced hexavalent chromium removal: morphology dependence of fibrillar vs particulate structures. Ind Eng Chem Res. 2017;56(38):10689–701.
2. Lytras G, Lytras C, Argyropoulou D, Dimopoulos N, Malavetas G, Lyberatos G. A novel two-phase bioreactor for microbial hexavalent chromium removal from wastewater. J Hazard Mater. 2017;336:41–51.
3. Fan S, Wang Y, Li Y, Tang J, Wang Z, Tang J, et al. Facile synthesis of tea waste/Fe 3 O 4 nanoparticle composite for hexavalent chromium removal from aqueous solution. RSC Adv. 2017;7(13):7576–90.
4. Habiba U, Siddique TA, Joo TC, Salleh A, Ang BC, Afifi AM. Synthesis of chitosan/polyvinyl alcohol/zeolite composite for removal of methyl orange, Congo red and chromium (VI) by flocculation/adsorption. Carbohydr Polym. 2017;157:1568–76.
5. Zhou L, Zhang G, Tian J, Wang D, Cai D, Wu Z. Functionalized Fe3O4@ C nanospheres with adjustable structure for efficient hexavalent chromium removal. ACS Sustain Chem Eng. 2017;5(11):11042–50.
6. I A, VA A, A B, CA M, GZ K. A review for chromium removal by carbon nanotubes. *Chemistry and Ecology*. 2017;**33**(6):572–88.
7. Lee C-G, Lee S, Park J-A, Park C, Lee SJ, Kim S-B, et al. Removal of copper, nickel and chromium mixtures from metal plating wastewater by adsorption with modified carbon foam. Chemosphere. 2017;166:203–11.
8. Zhan Y, He S, Wan X, Zhang J, Liu B, Wang J, et al. Easy-handling bamboo-like polypyrrole nanofibrous mats with high adsorption capacity for hexavalent chromium removal. J Colloid Interface Sci. 2018;529:385–95.
9. Li N, Tian Y, Zhao J, Zhang J, Zhang J, Zuo W, et al. Efficient removal of chromium from water by Mn3O4@ ZnO/Mn3O4 composite under simulated sunlight irradiation: synergy of photocatalytic reduction and adsorption. Appl Catal B Environ. 2017;214:126–36.
10. Gonçalves J, Santos J, Rios E, Crispim M, Dotto G, Pinto L. Development of chitosan based hybrid hydrogels for dyes removal from aqueous binary system. J Mol Liq. 2017;225:265–70.
11. Kallel F, Chaari F, Bouaziz F, Bettaieb F, Ghorbel R, Chaabouni SE. Sorption and desorption characteristics for the removal of a toxic dye, methylene blue from aqueous solution by a low cost agricultural by-product. J Mol Liq. 2016;219:279–88.
12. Ghadim EE, Manouchehri F, Soleimani G, Hosseini H, Kimiagar S, Nafisi S. Adsorption properties of tetracycline onto graphene oxide: equilibrium, kinetic and thermodynamic studies. PLoS One. 2013;8(11):e79254.
13. Fard RF, Sar MEK, Fahiminia M, Mirzaei N, Yousefi N, Mansoorian HJ, Khanjani N, Rezaei S, Ghadiri SK: Efficiency of multi walled carbon nanotubes for removing Direct Blue 71 from aqueous solutions. Eurasian J Anal Chem, **13**(3) 2018.
14. Robati D, Rajabi M, Moradi O, Najafi F, Tyagi I, Agarwal S, et al. Kinetics and thermodynamics of malachite green dye adsorption from aqueous solutions on graphene oxide and reduced graphene oxide. J Mol Liq. 2016;214:259–63.
15. Gao W, Alemany LB, Ci L, Ajayan PM. New insights into the structure and reduction of graphite oxide. Nat Chem. 2009;1(5):403–8.
16. Peng W, Li H, Liu Y, Song S. A review on heavy metal ions adsorption from water by graphene oxide and its composites. J Mol Liq. 2017;230:496–504.
17. Bhattacharyya A, Mondal D, Roy I, Sarkar G, Saha NR, Rana D, et al. Studies of the kinetics and mechanism of the removal process of Proflavine dye through adsorption by graphene oxide. J Mol Liq. 2017;230:696–704.
18. Ramesha G, Kumara AV, Muralidhara H, Sampath S. Graphene and graphene oxide as effective adsorbents toward anionic and cationic dyes. J Colloid Interface Sci. 2011;361(1):270–7.
19. Sun H, Cao L, Lu L. Magnetite/reduced graphene oxide nanocomposites: one step solvothermal synthesis and use as a novel platform for removal of dye pollutants. Nano Res. 2011;4(6):550–62.
20. Abdolhosseinzadeh S, Asgharzadeh H, Kim HS: Fast and fully-scalable synthesis of reduced graphene oxide. Sci Rep, 5.2015
21. Muramatsu H, Kim YA, Yang KS, Cruz-Silva R, Toda I, Yamada T, et al. Rice husk-derived Graphene with Nano-sized domains and clean edges. Small. 2014;10(14):2766–70.
22. Wang Z, Yu J, Zhang X, Li N, Liu B, Li Y, et al. Large-scale and controllable synthesis of Graphene quantum Dots from Rice husk biomass: a comprehensive utilization strategy. ACS Appl Mater Interfaces. 2016;8(2):1434–9.
23. Wang Y, Yang R, Wei Y, Zhao Z, Li M. Preparation of novel pigskin-derived carbon sheets and their low-temperature activation-induced high capacitive performance. RSC Adv. 2014;4(85):45318–24.
24. Pishgar-Komleh S, Sefeedpari P, Rafiee S. Energy and economic analysis of rice production under different farm levels in Guilan province of Iran. Energy. 2011;36(10):5824–31.
25. Ghaedi M, Khafri HZ, Asfaram A, Goudarzi A. Response surface methodology approach for optimization of adsorption of Janus green B from aqueous solution onto ZnO/Zn (OH) 2-NP-AC: kinetic and isotherm study. Spectrochim Acta A Mol Biomol Spectrosc. 2016;152:233–40.
26. Rakić T, Kasagić-Vujanović I, Jovanović M, Jančić-Stojanović B, Ivanović D. Comparison of full factorial design, central composite design, and box-Behnken Design in Chromatographic Method Development for the determination of fluconazole and its impurities. Anal Lett. 2014;47(8):1334–47.
27. Panahi AH, Ashrafi SD, Kamani H, Khodadadi M, Lima EC, Mostafapour FK, et al. Removal of cephalexin from artificial wastewater by mesoporous silica materials using box-Behnken response surface methodology. Desalin Water Treat. 2019;159:169–80.
28. Khazaei M, Nasseri S, Ganjali MR, Khoobi M, Nabizadeh R, Mahvi AH, et al. Modeling mercury (II) removal at ultra-low levels from aqueous solution using graphene oxide functionalized with magnetic nanoparticles: optimization, kinetics, and isotherm studies. Desalin Water Treat. 2017;83:144–58.
29. Khazaei M, Nasseri S, Ganjali MR, Khoobi M, Nabizadeh R, Mahvi AH, et al. Response surface modeling of lead ( ) removal by graphene oxide-Fe 3 O 4 nanocomposite using central composite design. J Environ Health Sci Eng. 2016;14(1):1.
30. Ashrafi S, Kamani H, Soheil Arezomand H, Yousefi N, Mahvi A. Optimization and modeling of process variables for adsorption of basic blue 41 on NaOH-modified rice husk using response surface methodology. Desalin Water Treat. 2016;57(30):14051–9.

31. Al-Musawi TJ, Kamani H, Bazrafshan E, Panahi AH, Silva MF, Abi G. Optimization the effects of physicochemical parameters on the degradation of cephalexin in sono-Fenton reactor by using box-Behnken response surface methodology. Catal Lett. 2019;149(5):1186–96.
32. Esfandiyari T, Nasirizadeh N, Ehrampoosh MH, Tabatabaee M. Characterization and absorption studies of cationic dye on multi walled carbon nanotube–carbon ceramic composite. J Ind Eng Chem. 2017;46:35–43.
33. Ghadiri SK, Nasseri S, Nabizadeh R, Khoobi M, Nazmara S, Mahvi AH. Adsorption of nitrate onto anionic bio-graphene nanosheet from aqueous solutions: isotherm and kinetic study. J Mol Liq. 2017;242:1111–7.
34. Nejat R, Chamack M, Mahjoub A. Active and recyclable ordered mesoporous magnetic organometallic catalyst as high-performance visible light photocatalyst for degradation of organic pollutants. Appl Organomet Chem. 2017;31(11):e3745.
35. Brunauer S, Emmett PH, Teller E. Adsorption of gases in multimolecular layers. J Am Chem Soc. 1938;60(2):309–19.
36. Jahangiri K, Yousefi N, Ghadiri SK, Fekri R, Bagheri A, Talebi SS: Enhancement adsorption of hexavalent chromium onto modified fly ash from aqueous solution; optimization; isotherm, kinetic and thermodynamic study. J Dispers Sci Technol:1–12.2018
37. Kontoyannis CG, Vagenas NV. Calcium carbonate phase analysis using XRD and FT-Raman spectroscopy. Analyst. 2000;125(2):251–5.
38. Buser C, Walther P. Freeze-substitution: the addition of water to polar solvents enhances the retention of structure and acts at temperatures around–60° C. J Microsc. 2008;230(2):268–77.
39. Rice EW, Baird RB, Eaton AD, Clesceri LS. Standard methods for the examination of water and wastewater, vol. 10. Washington, DC: American Public Health Association; 2012.
40. Eaton AD, Clesceri LS, Greenberg AE, Franson MAH. Standard methods for the examination of water and wastewater. American public health association. 2005;21:1600.
41. Terzioğlu P, Yucel S, Rabagah TM, Özçimen D. Characterization of wheat hull and wheat hull ash as a potential source of SiO2. BioResources. 2013;8(3):4406–20.
42. Zhang J, Yang H, Shen G, Cheng P, Zhang J, Guo S. Reduction of graphene oxide via L-ascorbic acid. Chem Commun. 2010;46(7):1112–4.
43. Li J, Li L, Zhang B, Yu M, Ma H, Zhang J, et al. Synthesis of few-layer reduced graphene oxide for lithium-ion battery electrode materials. Ind Eng Chem Res. 2014;53(34):13348–55.
44. Hyun Park J, Kim J-H. Reduction of graphene oxide by resveratrol: a novel and simple biological method for the synthesis of an effective anticancer nanotherapeutic molecule. Int J Nanomedicine. 2015;10:2951–69.
45. Pei S, Cheng H-M. The reduction of graphene oxide. Carbon. 2012;50(9):3210–28.
46. Wei Z, Pan R, Hou Y, Yang Y, Liu Y: Graphene-supported Pd catalyst for highly selective hydrogenation of resorcinol to 1, 3-cyclohexanedione through giant π-conjugate interactions. Sci Rep, 5.2015
47. Xu X, Gao B-Y, Yue Q-Y, Zhong Q-Q, Li Q. Preparation of new types of anion exchange resins from agricultural by-products and their utilization in the removal of various toxic anions from solutions. Chem Eng J. 2011;167(1):104–11.
48. Katal R, Baei MS, Rahmati HT, Esfandian H. Kinetic, isotherm and thermodynamic study of nitrate adsorption from aqueous solution using modified rice husk. J Ind Eng Chem. 2012;18(1):295–302.
49. Zhao G, Li J, Ren X, Chen C, Wang X. Few-layered graphene oxide nanosheets as superior sorbents for heavy metal ion pollution management. Environmental science & technology. 2011;45(24):10454–62.
50. Song W, Wang X, Wang Q, Shao D, Wang X. Plasma-induced grafting of polyacrylamide on graphene oxide nanosheets for simultaneous removal of radionuclides. Phys Chem Chem Phys. 2015;17(1):398–406.
51. Konkena B, Vasudevan S. Understanding aqueous dispersibility of graphene oxide and reduced graphene oxide through p K a measurements. The journal of physical chemistry letters. 2012;3(7):867–72.
52. Li D, Müller MB, Gilje S, Kaner RB, Wallace GG. Processable aqueous dispersions of graphene nanosheets. Nat Nanotechnol. 2008;3(2):101–5.
53. Ghadiri S, Nabizadeh R, Mahvi A, Nasseri S, Mesdaghinia A, Talebi S. Potential of granulated modified nanozeolites Y for MTBE removal from aqueous solutions: kinetic and isotherm studies. Pol J Chem Technol. 2012;14(2):1–8.
54. Najafabadi HH, Irani M, Rad LR, Haratameh AH, Haririan I. Removal of Cu2+, Pb2+ and Cr6+ from aqueous solutions using a chitosan/graphene oxide composite nanofibrous adsorbent. RSC Adv. 2015;5(21):16532–9.
55. Ghadiri S, Nabizadeh R, Mahvi A, Nasseri S, Kazemian H, Mesdaghinia A, et al. Methyl tert-butyl ether adsorption on surfactant modified natural zeolites. Iranian Journal of Environmental Health Science & Engineering. 2010;7(3):241.
56. Malakootian M, Moosazadeh M, Yousefi N, Fatehizadeh A. Fluoride removal from aqueous solution by pumice: case study on Kuhbonan water. Afr J Environ Sci Technol. 2011;5(4):299–306.
57. Mehrizi EA, Sadani M, Karimaei M, Ghahramani E, Ghadiri K, Taghizadeh MS. Isotherms and kinetics of lead and cadmium uptake from the waste leachate by natural absorbent. World Appl Sci J. 2011;15(12):1678–86.
58. Bazrafshan E, Balarak D, Panahi AH, Kamani H, Mahvi AH. Fluoride removal from aqueous solutions by cupricoxide nanoparticles. Fluoride. 2016;49(3):233.
59. Anastopoulos I, Anagnostopoulos VA, Bhatnagar A, Mitropoulos AC, Kyzas GZ. A review for chromium removal by carbon nanotubes. Chem Ecol. 2017;33(6):572–88.
60. Gholami Z, Ghadiri SK, Avazpour M, Fard MA, Yousefi N, Talebi SS, et al. Removal of phosphate from aqueous solutions using modified activated carbon prepared from agricultural waste (populous caspica): optimization, kinetic, isotherm, and thermodynamic studies. Desalin Water Treat. 2018;133:177–90.
61. Ghadiri SK, Alidadi H, Nezhad NT, Javid A, Roudbari A, Talebi SS, Mohammadi AA, Shams M, Rezania S (2020) Valorization of biomass into amine- functionalized bio graphene for efficient ciprofloxacin adsorption in water-modeling and optimization study. PLoS ONE 15(4). https://doi.org/10.1371/journal.pone.0231045